
CoSTI: Consistency Models for (a faster) Spatio-Temporal Imputation

Javier Solís-García¹ Belén Vega-Márquez¹ Juan A. Nepomuceno¹ Isabel A. Nepomuceno-Chamorro¹

Abstract

Multivariate Time Series Imputation (MTSI) is crucial for many applications, such as healthcare monitoring and traffic management, where incomplete data can compromise decision-making. Existing state-of-the-art methods, like Denoising Diffusion Probabilistic Models (DDPMs), achieve high imputation accuracy; however, they suffer from significant computational costs and are notably time-consuming due to their iterative nature. In this work, we propose CoSTI, an innovative adaptation of Consistency Models (CMs) for the MTSI domain. CoSTI employs Consistency Training to achieve comparable imputation quality to DDPMs while drastically reducing inference times, making it more suitable for real-time applications. We evaluate CoSTI across multiple datasets and missing data scenarios, demonstrating up to a 98% reduction in imputation time with performance on par with diffusion-based models. This work bridges the gap between efficiency and accuracy in generative imputation tasks, providing a scalable solution for handling missing data in critical spatio-temporal systems.

1. Introduction

One of the most pervasive challenges when working with Multivariate Time Series (MTS) is handling missing values. This issue, known as MTSI, is critical because inaccurate imputations can distort the original data distribution (Solís-García et al., 2023). Missing values arise from various situations, which differ across domains. For instance, they can result from sensor malfunctions in Internet of Things (IoT) applications, where this issue is common (Ahmed et al., 2022; Wu et al., 2020), or in clinical settings (Moor et al., 2020), where patient data may be irregularly recorded or omitted entirely.

MTSI has been extensively studied using traditional Ma-

chine Learning (ML) approaches (Moor et al., 2020; Chen et al., 2019) and, more recently, with advanced Deep Learning (DL) methods (Cao et al., 2018; Cini et al., 2022). Among these, generative models, particularly DDPMs (Ho et al., 2020), have achieved state-of-the-art results. However, diffusion models are computationally expensive, with prolonged inference times, making them impractical for many MTSI applications. In domains such as intensive care unit (ICU) patient monitoring (Solís-García et al., 2023), traffic flow control, air quality monitoring (Cini et al., 2022), and energy facility management (Sanchez-Lopez et al., 2024), where imputation is often a preprocessing step in multi-stage workflows, every second counts.

To address the inefficiency of diffusion models, a new type of techniques, **Consistency Models** (Song et al., 2023), has emerged. These models either distill diffusion models (*Consistency Distillation*) or train consistency models from scratch (*Consistency Training*) to achieve comparable quality in image generation while significantly reducing inference times.

In this work, we adapt this promising family of models to the MTSI domain by proposing *Consistency models for (a faster) Spatio-Temporal Imputation* (CoSTI). Our approach delivers imputation quality on par with DDPM-based models while drastically reducing imputation times. A representative schematic of the method is provided in Figure 1.

Our main contributions are as follows:

1. We introduce Consistency Models, trained through Consistency Training, for MTSI. To the best of our knowledge, this marks their first application in this domain.
2. We evaluate our model on four datasets across diverse domains and various missing-value scenarios, demonstrating a 98% reduction in imputation time compared to DDPM-based methods, with comparable performance.
3. We conduct extensive experiments to assess the model’s imputation quality and efficiency. To support reproducibility, we openly provide the code.

¹Dpto. Lenguajes y Sistemas Informáticos, University of Seville, Av. Reina Mercedes sn, Seville, 41012, Spain. Correspondence to: Javier Solís-García <jsolisg@us.es>.

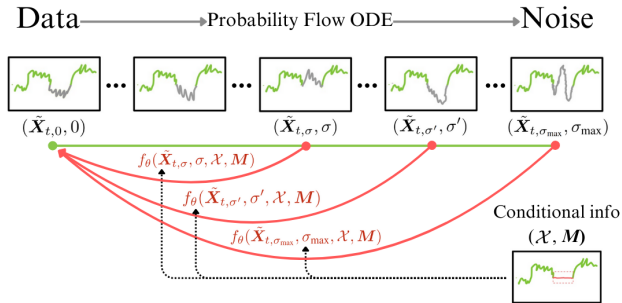


Figure 1. The objective is to map missing values back to their origin by leveraging a consistency model with conditional information. Given a Probability Flow ODE (PF-ODE) that progressively adds noise to the missing values, the model learns to reconstruct points along the ODE trajectory, allowing accurate imputations without the need for a full reverse path.

The rest of this paper is structured as follows: Section 2 reviews related work. Section 3 provides the mathematical foundations of our approach. Section 4 introduces CoSTI. Section 5 describes the experimental setup and results. Finally, Section 6 concludes the paper. Additional implementation details, code and results can be found in Appendices A and B, respectively.

2. Related Works

Multivariate time series imputation The challenge of MTSI has been extensively studied through a variety of approaches. Traditional methods, such as mean imputation, zero imputation, or linear trends (Moor et al., 2020), are simple to implement but often compromise data integrity by introducing bias. ML techniques, including k-nearest neighbors (Beretta & Santaniello, 2016), matrix factorization (Cichocki & Phan, 2009), and scalable Gaussian processes (Li & Marlin, 2016), offer more adaptive and robust solutions. DL further transformed the field with Recurrent Neural Networks (RNNs), which excel at capturing sequential dependencies critical for imputation tasks (Suo et al., 2019; Lipton et al., 2016). Bidirectional RNNs (BiRNNs), such as BRITS (Cao et al., 2018), enhance this capability by processing sequences in both forward and reverse temporal directions, allowing for more comprehensive temporal modeling.

Transformers, with their self-attention mechanisms, represent a significant step forward by addressing limitations of RNNs, such as error propagation, and efficiently capturing long-range dependencies in time series data (Tashiro et al., 2021; Liu et al., 2023). More recently, advances in generative models and State-Space Models (SSMs) have expanded the potential of MTSI methods. Structured State Space

Models (S4) (Gu et al., 2022) demonstrate strong sequence modeling capabilities, while attention-enhanced models like Selective State Space Models (S6) mitigate issues such as error accumulation. Mamba (Gu & Dao, 2023), an S6-based framework, has shown superior performance in sequence tasks, highlighting its promise for MTSI applications.

Generative methods have shown significant potential for MTSI due to their capacity to model complex data distributions. Early approaches, such as Variational Autoencoders (VAEs) (Fortuin et al., 2020) and Generative Adversarial Networks (GANs) (Miao et al., 2021), advanced the field but faced notable limitations. For instance, GANs often suffer from mode collapse (Thanh-Tung & Tran, 2020), which has shifted the focus toward more reliable generative frameworks. Moreover, the integration of Graph Neural Networks (GNNs) with temporal models has further enhanced imputation by effectively capturing spatial relationships inherent in multivariate data (Cini et al., 2022; Liu et al., 2023). These developments highlight not only the rapid evolution of MTSI methodologies but also the untapped potential of combining recent innovations, paving the way for increasingly accurate, scalable, and robust imputation frameworks

Diffusion models for MTSI DDPMs have emerged as a robust solution for MTSI, leveraging iterative denoising processes to reconstruct missing data with high accuracy. Conditioning mechanisms, as demonstrated by CSDI (Tashiro et al., 2021), are critical to their success, allowing DDPMs to outperform earlier generative methods. Conversely, unconditional DDPMs fail to deliver accurate imputations (Yun et al., 2023), underscoring the importance of carefully crafted conditional architectures. Recent advancements, such as PriSTI (Liu et al., 2023), have refined this approach by introducing specialized layers to enhance the generation of conditional information, achieving state-of-the-art results. Furthermore, the integration of S4 blocks into DDPMs has shown promise in improving temporal modeling efficiency (Alcaraz & Strodtzoff, 2023).

Recent advancements have further demonstrated the flexibility of DDPM architectures. TIMBA (Solís-García et al., 2024), for instance, replaces Transformer-based temporal blocks with bidirectional Mamba blocks, achieving competitive performance and showcasing the effectiveness of structured attention mechanisms in diffusion models. This approach highlights how architectural adaptations can further enhance the robustness and efficiency of DDPMs for MTSI, reinforcing their status as a leading framework for accurate and reliable time series imputation.

Consistency models Consistency Models (CMs) are a recent advancement in generative modeling, closely related to DDPMs, but designed to optimize for single-step generation. This approach prioritizes faster inference, albeit with a

potential trade-off in generation quality. CMs can be developed either through *Consistency Distillation* (CD), where a diffusion model is distilled into a single-step generator, or trained independently using *Consistency Training* (CT) (Song et al., 2023).

Initially, CMs excelled in speed but struggled to match the quality of diffusion models. Over time, refined methodologies and implementations have significantly bridged this gap, enabling CMs to achieve performance comparable to state-of-the-art diffusion models. While CD has historically been the dominant training paradigm, it involves training a diffusion model as an intermediate step, increasing computational cost. Recent advancements have demonstrated that CT can surpass CD in performance while eliminating the need for an intermediary diffusion model, reducing both training time and resource requirements (Song & Dhariwal, 2024; Geng et al., 2024; Lu & Song, 2024).

Despite their potential, CMs remain underexplored due to their relatively recent introduction. Current applications are largely confined to computer vision, where approaches such as Latent Consistency Models (Luo et al., 2023) have leveraged Latent Diffusion Models (Rombach et al., 2022) to achieve faster generation speeds without compromising output quality. However, to the best of our knowledge, CMs have yet to be applied to time series data or MTSI, presenting a promising opportunity to exploit their rapid generation capabilities in this domain.

3. Background

3.1. Multivariate Time Series Imputation

A MTS consists of recordings at different time steps, denoted by t , across multiple variables or channels, denoted by N_t . Formally, an MTS can be represented as $\mathbf{X}_t \in \mathbb{R}^{N_t \times d}$, where each row i contains the d -dimensional vector $\mathbf{x}_t^i \in \mathbb{R}^d$, corresponding to the i -th variable at time t . Additionally, a binary mask matrix $\mathbf{M}_t \in \{0, 1\}^{N_t \times d}$ is used to indicate the presence of missing values: $\mathbf{M}_t[i, j] = 0$ when the corresponding value in \mathbf{X}_t is missing, and $\mathbf{M}_t[i, j] = 1$ when the value is observed.

The imputed time series generated by a model is represented as $\hat{\mathbf{X}}_t$, while $\tilde{\mathbf{X}}_t$ and \mathbf{X}_t denote the data with missing values and ground-truth imputation we aim to approximate, and \mathcal{X}_t refers to the time series imputed using a linear interpolation technique.

Since our approach leverages graph-based models, following Cini et al. (2022), we model the MTS as a sequence of graphs. At each time step t , a graph $\mathcal{G}_t = \langle \tilde{\mathbf{X}}_t, \mathcal{A}_t \rangle$ is defined, where \mathcal{A}_t is the adjacency matrix for that time step. In this work, we assume a constant graph topology over time; thus, \mathcal{A} remains fixed for all t .

3.2. Consistency Models

CMs are built on the probability flow ordinary differential equation (PF-ODE), which describes the evolution of data corrupted by Gaussian noise. Starting from a data distribution $p_{\text{data}}(\mathbf{x})$, the diffusion process applies noise perturbations $\mathcal{N}(0, \sigma)$, transforming the data into pure noise. This process is expressed as (Song & Dhariwal, 2024):

$$p_\sigma(\mathbf{x}) = \int p_{\text{data}}(\mathbf{y}) \mathcal{N}(\mathbf{x}|\mathbf{y}, \sigma^2 \mathbf{I}) d\mathbf{y} \quad (1)$$

The PF-ODE is given by (Karras et al., 2022):

$$\frac{d\mathbf{x}}{d\sigma} = -\sigma \nabla_x \log p_\sigma(\mathbf{x}) \quad \sigma \in [\sigma_{\min}, \sigma_{\max}] \quad (2)$$

where $\nabla_x \log p_\sigma(\mathbf{x})$, referred to as the score function, measures the gradient of the log-likelihood of the data under $p_\sigma(\mathbf{x})$. Diffusion models are a type of *score-based generative model* because they estimate this score function at different noise levels during the corruption process (Song et al., 2021). For practical implementation, σ_{\min} is set to a small value such that $p_{\sigma_{\min}}(\mathbf{x}) \approx p_{\text{data}}(\mathbf{x})$, and σ_{\max} is large enough to approximate $p_{\sigma_{\max}}(\mathbf{x}) \sim \mathcal{N}(0, \sigma_{\max}^2 \mathbf{I})$. Following Karras et al. (2022), we set $\sigma_{\min} = 0.002$ and $\sigma_{\max} = 80$.

The PF-ODE allows transitioning between noise levels. For example, $\mathbf{x}_{\sigma_{\min}}$ can be recovered from \mathbf{x}_σ by solving the PF-ODE, defining a *consistency function* $\mathbf{f}^* : (\mathbf{x}_\sigma, \sigma) \rightarrow \mathbf{x}_{\sigma_{\min}}$. This function must satisfy *self-consistency*: $\mathbf{f}^*(\mathbf{x}_\sigma, \sigma) = \mathbf{f}^*(\mathbf{x}_{\sigma'}, \sigma')$ for any $\sigma, \sigma' \in [\sigma_{\min}, \sigma_{\max}]$. Additionally, it must respect the *boundary condition* $\mathbf{f}^*(\mathbf{x}, \sigma_{\min}) = \mathbf{x}$, where it acts as an identity function (Song et al., 2023).

The consistency function is parameterized using a neural network called the *consistency model*, \mathbf{f}_θ , which is designed to approximate \mathbf{f}^* while adhering to the boundary condition. The parameterization used in this work, following Song et al. (2023), is:

$$\mathbf{f}_\theta(\mathbf{x}, \sigma) = c_{\text{skip}}(\sigma) \mathbf{x} + c_{\text{out}}(\sigma) \mathbf{F}_\theta(\mathbf{x}, \sigma) \quad (3)$$

With differentiable functions $c_{\text{skip}}(\sigma)$ and $c_{\text{out}}(\sigma)$ such that $c_{\text{skip}}(\sigma_{\min}) = 1$ and $c_{\text{out}}(\sigma_{\min}) = 0$, defined as:

$$c_{\text{skip}}(\sigma) = \frac{\sigma_{\text{data}}^2}{(\sigma - \sigma_{\min}) + \sigma_{\text{data}}^2}, \quad c_{\text{out}}(\sigma) = \frac{\sigma_{\text{data}}^2 (\sigma - \sigma_{\min})}{\sqrt{\sigma_{\text{data}}^2 + \sigma^2}} \quad (4)$$

Training involves discretizing the PF-ODE into noise levels $\sigma_{\min} = \sigma_1 < \dots < \sigma_N = \sigma_{\max}$, parameterized as $\sigma_i = (\sigma_{\min}^{1/\rho} + \frac{i-1}{N-1} (\sigma_{\max}^{1/\rho} - \sigma_{\min}^{1/\rho}))^\rho$ with $\rho = 7$ (Karras et al., 2022).

The training objective minimizes the *consistency matching* loss:

$$\mathcal{L}^N(\boldsymbol{\theta}, \boldsymbol{\theta}^-) = \mathbb{E}[\lambda(\sigma_i)d(\mathbf{f}_{\boldsymbol{\theta}}(\mathbf{x}_{\sigma_{i+1}}, \sigma_{i+1}), \mathbf{f}_{\boldsymbol{\theta}^-}(\mathbf{x}_{\sigma_i}, \sigma_i))] \quad (5)$$

where $d(\mathbf{x}, \mathbf{y})$ is the Pseudo-Huber metric (Charbonnier et al., 1997), $d(\mathbf{x}, \mathbf{y}) = \sqrt{\|\mathbf{x} - \mathbf{y}\|_2^2 + c^2} - c$, with $c = 0.00054\sqrt{d}$, and $\lambda(\sigma) = 1/(\sigma_{i+1} - \sigma_i)$. In this framework, $\mathbf{f}_{\boldsymbol{\theta}}$ is the *student network*, while $\mathbf{f}_{\boldsymbol{\theta}^-}$ is the *teacher network*. Both networks share the same parameters, but during training, $\mathbf{f}_{\boldsymbol{\theta}^-}$ executes its forward pass using a `stopgrad` operation, preventing gradient computation for this network and ensuring stability. Noise levels i are sampled using a discrete Lognormal distribution parameterized as $i \sim p(i) \propto \text{erf}(\frac{\log(\sigma_{i+1} - P_{\text{mean}})}{\sqrt{2}P_{\text{std}}}) - \text{erf}(\frac{\log(\sigma_i - P_{\text{mean}})}{\sqrt{2}P_{\text{std}}})$, where $P_{\text{mean}} = -1.1$ and $P_{\text{std}} = 2.0$ (Song & Dhariwal, 2024).

4. CoSTI

4.1. Consistency Training for imputation

To train a Consistency Model for MTSI, we introduced several modifications to improve the results. Below, we detail the adjustments made and describe the final architecture used to implement the Consistency Model. More comprehensive information on the training and sampling procedures can be found in Algorithms 1 and 2 in the Appendix A.1.

4.1.1. CONDITIONAL INFORMATION

Consistency models share many similarities with diffusion models, as they are heavily inspired by the underlying theoretical framework. Diffusion models have been successfully applied in the field of MTSI, often emphasizing the importance of incorporating enhanced conditional information to guide the model towards better imputations. Indeed, Yun et al. (2023) demonstrated that without this conditional information, these models fail to produce adequate imputations.

In light of these findings and building on the successes of diffusion-based models in this domain, we incorporated conditional information following a philosophy similar to Liu et al. (2023). Specifically, we included $\mathcal{X}_t, \mathcal{A}, \mathbf{M}_t$. Consequently, our Consistency Model is parameterized as follows: $F_{\boldsymbol{\theta}} : (\mathbf{X}_{t, \sigma_i}, \mathcal{X}_t, \mathcal{A}, \mathbf{M}_t, \sigma_i) \rightarrow \hat{\mathbf{X}}_t$.

4.1.2. LOSS FUNCTION AND REGULARIZATION

In MTSI, the task requires reconstructing information often entirely absent in the original dataset. To simulate this scenario during training, synthetic missing values are dynamically generated in each batch. The error is then computed solely at positions where ground-truth information exists. This process yields $\tilde{\mathbf{X}}_t$, a data matrix with synthetic missing

values, and $\tilde{\mathbf{M}}_t$, an updated mask matrix reflecting these values. Incorporating these updates and the conditional information from Section 4.1.1, the loss function is defined as:

$$\mathcal{L}^N(\boldsymbol{\theta}, \boldsymbol{\theta}^-) = \mathbb{E}[\mathbf{M} \cdot \lambda(\sigma_i)d(\mathbf{f}_{\boldsymbol{\theta}}(\tilde{\mathbf{X}}_{t, \sigma_{i+1}}, \mathcal{X}_t, \mathcal{A}, \tilde{\mathbf{M}}_t, \sigma_{i+1}), \mathbf{f}_{\boldsymbol{\theta}^-}(\tilde{\mathbf{X}}_{t, \sigma_i}, \mathcal{X}_t, \mathcal{A}, \tilde{\mathbf{M}}_t, \sigma_i))] \quad (6)$$

Additionally, strong regularization is critical for CMs. We observed that increasing the dropout rate from 0.1 (common in prior work (Tashiro et al., 2021; Liu et al., 2023; Solís-García et al., 2024)) to 0.2 improved performance, underscoring the importance of mitigating overfitting during training. This adjustment, along with synthetic missing values, enhances the model’s robustness in handling diverse imputations.

4.1.3. OPTIMIZATION STRATEGY AND CURRICULUM LEARNING

Optimization strategies in prior work have varied. Song et al. (2023) and Song & Dhariwal (2024) used RAdam without schedulers or weight decay, while Geng et al. (2024) incorporated learning rate decay in their experiments with RAdam and Adam. In our approach, we adopted the Scheduler-Free optimizer (Defazio et al., 2024), specifically the AdamW variant, which eliminates the need for a learning rate scheduler while achieving state-of-the-art results. To ensure stable convergence, we introduced weight decay, further emphasizing the role of regularization in training Consistency Models.

For curriculum learning, we progressively increased N during training to refine consistency across different σ values. This strategy allows the model to start by comparing points farther apart along the PF-FLOW and gradually focus on smaller differences between closer σ values (Song & Dhariwal, 2024). In this work, we used a linear scheduler, incrementing N from $s_0 = 10$ to $s_1 = 200$, achieving a balance between simplicity and effective training.

4.1.4. DETERMINISTIC IMPUTATION

Like diffusion models, Consistency Models generate probabilistic imputations. To produce a deterministic result, we performed 100 imputations, estimated the distribution of predicted values, and used the median as the final output. This approach, as described in (Tashiro et al., 2021), ensures a robust and consistent result suitable for practical applications.

4.2. Model architecture

Our model’s architecture is primarily inspired by the U-Net structure (Ronneberger et al., 2015), a design extensively adopted in various works exploring consistency models (Song et al., 2023; Song & Dhariwal, 2024; Luo et al., 2023). However, recent advancements in the application of DDPMs to MTSI have introduced specialized components tailored to the problem (Tashiro et al., 2021; Liu et al., 2023; Solís-García et al., 2024). In this work, we propose a hybrid approach, combining the foundational principles of U-Net with adaptations informed by recent developments in the literature. This architecture is both validated by prior research and designed to leverage the strengths of consistency models. A high-level overview of the proposed architecture is presented in Figure 2.

4.2.1. SPATIO-TEMPORAL FEATURE EXTRACTION MODULES (STFEM)

An essential component of our model is the Spatio-Temporal Feature Extraction Module (STFEM), which extends the design principles of the Conditional Feature Extraction Modules proposed in prior work (Liu et al., 2023). STFEMs are specifically crafted to extract spatio-temporal representations by combining bidirectional Mamba blocks, transformers with self-attention for spatial dimensions, and a Message Passing Neural Network inspired by Wu et al. (2019b). The architecture incorporates two STFEMs corresponding to the model’s dual input streams: the primary input channel ($\mathbf{X}_t, \mathcal{A}$), located in the upper branch of Figure 2, and the conditional information channel, positioned in the lower branch, which processes inputs ($\mathcal{X}_t, \mathbf{M}_t, \mathcal{A}$).

4.2.2. U-NET COMPRESSION AND CROSS-ATTENTION

Following STFEM, both branches of the model proceed through the compression stage of the U-Net architecture. Temporal and spatial dimensions are sequentially reduced by factors f_t and f_s , respectively. This follows the “time-then-graph” approach (Gao & Ribeiro, 2022), utilizing blocks specifically designed for each dimension and comprising transformers and convolutional layers.

In the conditional branch, information is compressed using self-attention, generating representations at three stages to serve as conditional inputs. In the primary branch, compression employs cross-attention mechanisms to incorporate conditional information. Specifically, in each attention block, the primary sequence $\mathbf{Z} \in \mathbb{R}^{n \times d}$ and the conditional sequence $\mathbf{H} \in \mathbb{R}^{n \times d}$ are combined using the attention mechanism defined as $\text{Attention}(\mathbf{Q}, \mathbf{K}, \mathbf{V}) = \text{softmax}\left(\frac{\mathbf{Q}\mathbf{K}^T}{\sqrt{d}}\right) \cdot \mathbf{V}$, where $\mathbf{Q} = \mathbf{W}_Q^{(i)} \cdot \mathbf{Z}$, $\mathbf{K} = \mathbf{W}_K^{(i)} \cdot \mathbf{H}$, and $\mathbf{V} = \mathbf{W}_V^{(i)} \cdot \mathbf{H}$, with $\mathbf{W}_Q^{(i)}, \mathbf{W}_K^{(i)}, \mathbf{W}_V^{(i)} \in \mathbb{R}^{d \times d}$ (Rombach et al., 2022).

4.2.3. NOISE EXTRACTION MODULES (NEM)

At the bottleneck of the U-Net, Noise Extraction Modules (NEM) are employed, following their introduction by Tashiro et al. (2021) and subsequent enhancements by Liu et al. (2023) and Solís-García et al. (2024). Originally designed for estimating noise in diffusion models, we adapt NEMs for consistency models, leveraging the conditional information extracted earlier.

These modules integrate bidirectional Mamba blocks in place of temporal transformers, as in (Solís-García et al., 2024). However, given Mamba blocks’ lack of native support for cross-attention, we reintroduce transformers for this purpose. Each NEM comprises the following sequence: a temporal transformer with cross-attention for conditional information, a bidirectional Mamba block for sequence analysis, a spatial transformer with cross-attention, and a spatial transformer with self-attention. This design ensures that both temporal and spatial dimensions are analyzed for conditional and intrinsic sequence data.

Finally, the outputs are processed through a Multi-Layer Perceptron (MLP) with gated activation. Each NEM produces two outputs: one as input for the next NEM and another as a noise estimate, H_{NEM_i} . Each block also incorporates an embedding for σ , constructed using positional embeddings (Song & Dhariwal, 2024).

4.2.4. FINAL RECONSTRUCTION

After summing the noise estimates (H_{NEM_i}), the data passes through the reconstruction stage of the U-Net, which restores the original dimensionality of the inputs. This process leverages the conditional information and utilizes skip connections to integrate features from the initial stages of the architecture.

5. Experiments

5.1. Datasets

To evaluate our approach, we use datasets that are well-established and frequently cited in the literature, but at the same time serve to represent the importance of obtaining faster imputations.

We used datasets identical to those in Cini et al. (2022), which established benchmarks subsequently adopted as comparison metrics. Specifically, the **AQI-36** dataset (Yi et al., 2016) contains hourly air quality readings from 36 stations in Beijing over one year, with 13.24% missing data. Additionally, we used the **METR-LA** and **PEMS-BAY** datasets (Li et al., 2018), which document traffic conditions in Los Angeles and San Francisco Bay Area, respectively. METR-LA includes records from 207 sensors over four months with an 8.10% missing rate, while PEMS-BAY comprises

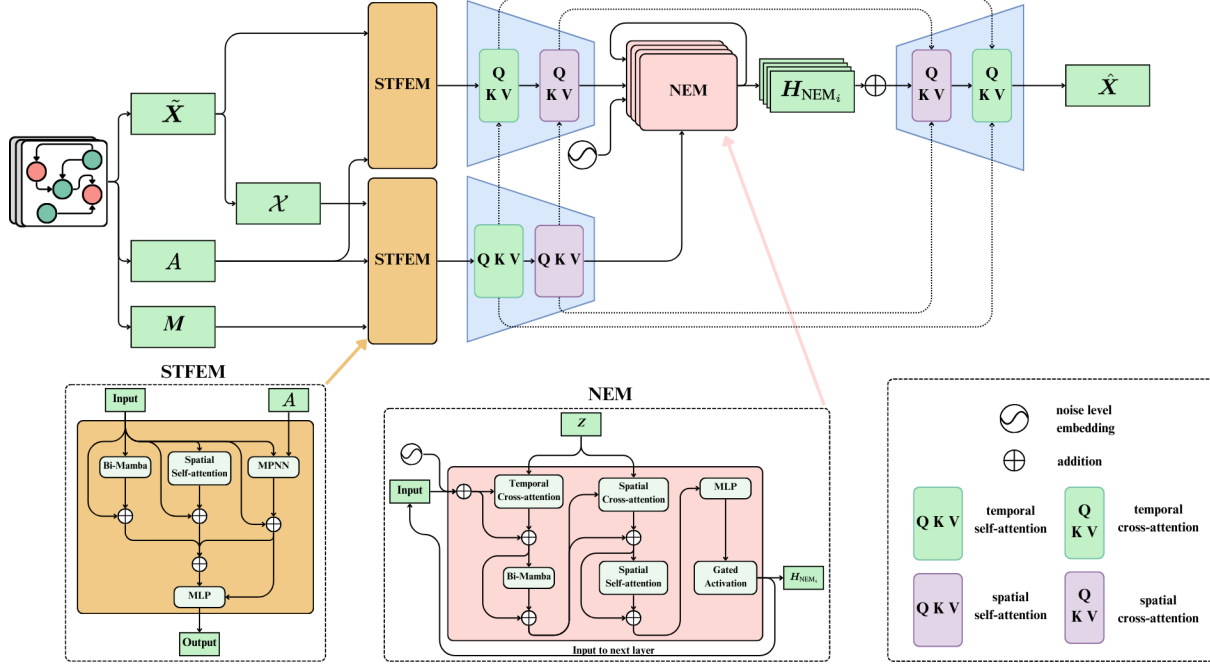


Figure 2. Graphical representation of the architecture implemented in CoSTI. The figure illustrates the two information channels (primary and conditional), the internal structure of the U-Net, and the details of the STFEM and NEM blocks.

data from 325 sensors over six months, with only 0.02% missing values. These datasets exemplify situations where fast imputation is critical: air quality monitoring ensures timely health alerts, and traffic analysis enables real-time route optimization.

In line with the benchmark, we replicated adjacency matrices using thresholded Gaussian Kernels based on geographical distances, as proposed by Wu et al. (2019a). The original data splits (70% training, 10% validation, 20% testing) and random seeds were maintained. For AQI-36, testing occurred in February, May, August, and November, as originally defined, with a 10% validation sample drawn using the same seed.

We also incorporated data from the **PhysioNet Challenge 2019** (Reyna et al., 2019), which includes clinical records for 40,336 ICU patients from two hospitals. This dataset, aimed at early detection of sepsis, features 40 variables per patient, including vital signs, lab results, and demographic information. Fast imputations are essential in this context, as missing clinical data can delay critical decisions in ICUs. Sepsis requires rapid intervention to reduce mortality, making efficient imputation vital for real-time risk assessments. Following Solís-García et al. (2023), we allocated 80% of the data for training, 10% for validation, and 10% for testing. Adjacency matrices were constructed by computing correlations between variables.

To evaluate imputation performance, we generated synthetic

missing data in three scenarios: (1) “Block missing” simulates missing data in 5% of the samples and masks 1–4-hour blocks at a probability of 0.15% for each sensor; (2) “Point missing” randomly masks 25% of values; and (3) a scenario where missing values match the original data distribution.

5.2. Experimental settings

All experiments were conducted five times with different random seeds to ensure robustness. Four synthetic missing data generation strategies were employed during the training:

- 1) **Point Strategy:** Randomly masks [0, 100]% of data per batch.
- 2) **Block Strategy:** Generates sequences of missing values of length $[L/2, L]$ with a [0, 15]% probability, alongside an additional 5% random missingness.
- 3) **Historical Strategy:** Uses original imputation masks from the dataset.
- 4) **Hybrid Strategy:** Combines the point strategy (primary) with either the block or historical strategy (secondary) with a 50% probability.

For “Point missing” scenarios, the point strategy was applied. “Block missing” scenarios utilized the hybrid strategy with the block strategy as secondary. For AQI-36, the hybrid strategy was employed with the historical strategy as secondary. Finally, the PhysioNet Challenge 2019 dataset was trained using the point strategy.

Training epochs varied by dataset: 200 for AQI-36, 300

for METR-LA, 150 for PEMS-BAY, and 50 for PhysioNet Challenge 2019. Results for CSDI, PriSTI, and TIMBA were sourced from Solís-García et al. (2024), except for the PhysioNet Challenge 2019, where experiments were conducted to obtain comparable results.

Detailed hyperparameters and reproducibility information are provided in Appendix A.2.

5.3. Results and Discussion

5.3.1. PERFORMANCE ANALYSIS: IMPUTATION RESULTS

Table 1 reports the inference times (in hours) required to impute the test sets of the evaluated datasets for all considered diffusion models and CoSTI using a single sampling step. Additionally, Tables 2 and 3 present the imputation performance of CoSTI with 1 and 2 sampling steps (denoted as CoSTI and CoSTI-2, respectively) compared to other diffusion models across all datasets and experimental scenarios described in Section 5.2.

Table 1. Time in hours required to impute the test set for each dataset using each model. The fastest time is highlighted in bold.

Dataset	CSDI	PriSTI	TIMBA	CoSTI
AQI-36	0.22	0.33	0.44	0.005
METR-LA	1.74	2.44	3.65	0.06
PEMS-BAY	4.62	5.99	8.71	0.16
Physionet	8.16	15.86	18.19	0.48

Table 2. Results obtained by applying the models to the AQI-36 and PhysioNet Challenge 2019 datasets with additional synthetic missing values. The best value is highlighted in bold, and any case where CoSTI outperforms a DDPM model is underlined.

Models	AQI-36		Physionet Challenge 2019	
	Simulated failure (24.6%)		Simulated failure (83.82%)	
	MAE	MSE	MAE	MSE
CSDI	9.74 ± 0.16	388.37 ± 11.42	3.93 ± 0.76	2282.94 ± 2646.26
PriSTI	9.84 ± 0.11	376.11 ± 10.62	3.58 ± 0.33	573.06 ± 22.89
TIMBA	9.56 ± 0.4	352.29 ± 5.33	3.11 ± 0.32	521.29 ± 23.11
CoSTI	10.13 ± 0.08	<u>377.48</u> ± 9.29	<u>2.47</u> ± 0.05	<u>388.31</u> ± 36.55
CoSTI-2	9.90 ± 0.13	<u>358.67</u> ± 13.05	<u>2.46</u> ± 0.07	<u>334.40</u> ± 23.84

Inference Speed Analysis: From Table 1, it is evident that CoSTI significantly outperforms diffusion models in terms of inference speed. Unlike CSDI, PriSTI, and TIMBA, which require T steps to generate a sample from noise, CoSTI achieves sampling with just one step. This characteristic makes CoSTI approximately $1/T$ times faster than the other models. For AQI-36, diffusion models use $T = 100$, while for other datasets, $T = 50$, which aligns with the observed results: CoSTI requires only 1.64% of TIMBA’s

time for imputing METR-LA and 0.91% for AQI-36. All experiments were conducted on an NVIDIA RTX A5000 24 GB GPU; further details on hardware and implementation requirements are provided in Appendix A.

Imputation Accuracy Analysis: Tables 2 and 3 highlight that although CoSTI does not consistently achieve the best results, its performance is comparable to that of CSDI, PriSTI, and TIMBA. Notably, CoSTI excels in the Physionet Challenge 2019 dataset. Furthermore, increasing the number of sampling steps enhances CoSTI’s accuracy, as shown by the improvements observed with CoSTI-2. This demonstrates a trade-off between speed and performance, offering flexibility depending on application needs.

For a more exhaustive analysis of the models, Appendix B includes ablation studies, modifications to CoSTI’s training, and a comparison against a well-established benchmark in the literature. These additional experiments provide deeper insights into the model’s behavior under various configurations and further contextualize its performance.

5.3.2. SENSITIVITY ANALYSIS

To evaluate sensitivity to varying missing value ratios, we tested CoSTI, CSDI, PriSTI, and TIMBA on the METR-LA dataset under the Point-missing scenario with different levels of missing data. Leveraging the best-performing model weights from Table 3, the results are visualized in Figure 3. CoSTI exhibits performance comparable to PriSTI and TIMBA, particularly under higher missing rates, underscoring its robustness and reliability in challenging imputation scenarios.

5.3.3. DOWNSTREAM TASK EVALUATION

Assessing imputation models solely on reconstruction metrics may not reflect their practical utility. Thus, we evaluate their effectiveness on a downstream task: node value prediction. This task, consistent with Solís-García et al. (2024), involves predicting a node’s value at time t using values from other nodes at the same timestamp.

Using the AQI-36 dataset, missing values were imputed with the best-performing model weights from Table 2. Imputed data were split into a new training (80%) and test set (20%), normalized with a MinMax scaler. We trained an MLP with one hidden layer (100 neurons) for 500 epochs, minimizing MSE. Final test metrics excluded imputed target values, focusing on actual values only. As seen in Table 4, CoSTI achieves comparable performance to diffusion-based models, outperforming them in node 31 prediction.

Table 3. Results obtained by applying the models to the METR-LA and PEMS-BAY datasets under the ‘‘Point missing’’ and ‘‘Block missing’’ scenarios. The best value is highlighted in bold, and any case where CoSTI outperforms a DDPM model is underlined.

Models	METR-LA				PEMS-BAY			
	Block-missing (16.6%)		Point-missing (31.1%)		Block-missing (9.2%)		Point-missing (25.0%)	
	MAE	MSE	MAE	MSE	MAE	MSE	MAE	MSE
CSDI	1.90 ± 0.01	12.27 ± 0.18	1.77 ± 0.05	9.42 ± 0.47	0.84 ± 0.00	4.06 ± 0.04	0.58 ± 0.00	1.30 ± 0.04
PriSTI	1.78 ± 0.00	10.64 ± 0.13	1.70 ± 0.00	8.47 ± 0.04	0.87 ± 0.01	4.64 ± 0.21	0.59 ± 0.00	1.61 ± 0.03
TIMBA	1.76 ± 0.02	10.36 ± 0.34	1.69 ± 0.00	8.36 ± 0.01	0.84 ± 0.01	4.57 ± 0.08	0.58 ± 0.00	1.63 ± 0.08
CoSTI	<u>1.85</u> ± 0.01	<u>11.44</u> ± 0.08	<u>1.76</u> ± 0.01	<u>9.01</u> ± 0.06	0.93 ± 0.03	<u>4.52</u> ± 0.15	0.64 ± 0.01	<u>1.53</u> ± 0.15
CoSTI-2	<u>1.84</u> ± 0.01	<u>11.35</u> ± 0.14	<u>1.75</u> ± 0.00	<u>8.97</u> ± 0.05	0.91 ± 0.02	<u>4.43</u> ± 0.12	0.63 ± 0.01	<u>1.44</u> ± 0.12

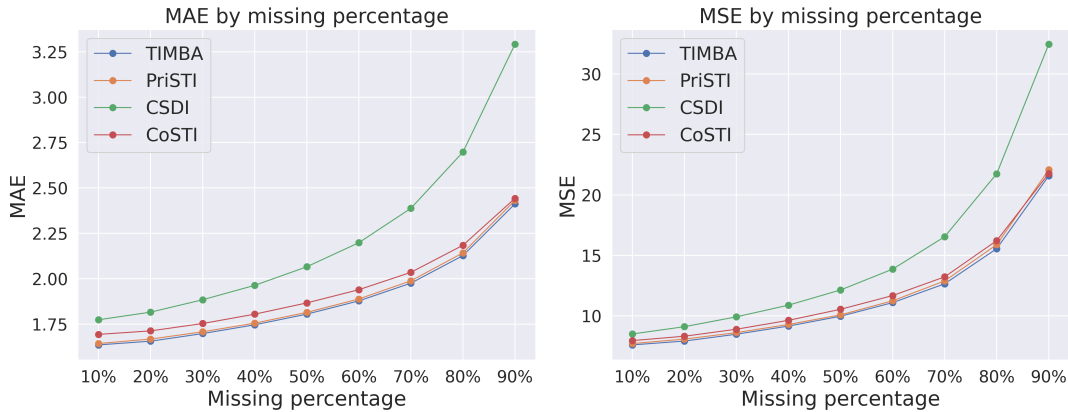


Figure 3. Graphs showing the performance of the models under different missing value ratios. Since PriSTI and TIMBA overlap significantly, making them harder to distinguish, a more detailed version in graphical form can be found in Appendix B.

Table 4. Performance results for the downstream task of node value prediction using data imputed by the evaluated models. The best value is highlighted in bold, and any case where CoSTI outperforms a DDPM model is underlined.

Models	Sensor 14		Sensor 31	
	MAE	MSE	MAE	MSE
CSDI	6.51 ± 0.69	96.99 ± 21.25	11.99 ± 1.92	376.40 ± 148.06
PriSTI	6.46 ± 0.71	92.70 ± 20.27	11.70 ± 1.80	361.19 ± 132.99
TIMBA	6.45 ± 0.69	91.90 ± 20.33	11.68 ± 1.77	359.80 ± 131.74
CoSTI	<u>6.51</u> ± 0.67	<u>93.96</u> ± 20.60	<u>11.41</u> ± 1.88	<u>350.46</u> ± 135.60

6. Conclusions

This work introduced CoSTI, a novel model for MTSI that leverages Consistency Models to achieve results comparable to state-of-the-art diffusion-based methods, while drastically reducing computational costs. By incorporating Consistency Training, CoSTI demonstrated up to a 98% reduction in inference time across diverse datasets and missing data scenarios.

These results position CoSTI as an efficient and scalable solution for real-time applications in critical domains like

healthcare and traffic management. Future work could explore adapting CoSTI for time series forecasting and further optimizing training efficiency through Latent Consistency Models.

Impact Statement

This paper presents work whose goal is to advance the field of Machine Learning. There are many potential societal consequences of our work, none which we feel must be specifically highlighted here.

References

- Ahmed, H. M., Abdulrazak, B., Blanchet, F. G., Aloulou, H., and Mokhtari, M. Long gaps missing iot sensors time series data imputation: A bayesian gaussian approach. *IEEE Access*, 10:116107–116119, 2022.
- Alcaraz, J. L. and Strodthoff, N. Diffusion-based time series imputation and forecasting with structured state space models. *Transactions on Machine Learning Research*, 2023. ISSN 2835-8856. URL <https://openreview.net/forum?id=hHiIbk7ApW>.

- Beretta, L. and Santaniello, A. Nearest neighbor imputation algorithms: a critical evaluation. *BMC medical informatics and decision making*, 16(3):197–208, 2016.
- Cao, W., Wang, D., Li, J., Zhou, H., Li, L., and Li, Y. Brits: Bidirectional recurrent imputation for time series. *Advances in neural information processing systems*, 31, 2018.
- Charbonnier, P., Blanc-Féraud, L., Aubert, G., and Barlaud, M. Deterministic edge-preserving regularization in computed imaging. *IEEE Transactions on image processing*, 6(2):298–311, 1997.
- Chen, X., He, Z., Chen, Y., Lu, Y., and Wang, J. Missing traffic data imputation and pattern discovery with a bayesian augmented tensor factorization model. *Transportation Research Part C: Emerging Technologies*, 104: 66–77, 2019.
- Cichocki, A. and Phan, A.-H. Fast local algorithms for large scale nonnegative matrix and tensor factorizations. *IEICE transactions on fundamentals of electronics, communications and computer sciences*, 92(3):708–721, 2009.
- Cini, A. and Marisca, I. Torch Spatiotemporal, 3 2022. URL <https://github.com/TorchSpatiotemporal/tsl>.
- Cini, A., Marisca, I., and Alippi, C. Filling the g_{ap}s: Multivariate time series imputation by graph neural networks. In *International Conference on Learning Representations*, 2022. URL <https://openreview.net/forum?id=kOu3-S3wJ7>.
- Defazio, A., Yang, X. A., Khaled, A., Mishchenko, K., Mehta, H., and Cutkosky, A. The road less scheduled. In *The Thirty-eighth Annual Conference on Neural Information Processing Systems*, 2024. URL <https://openreview.net/forum?id=0XeNkkENuI>.
- Falcon, W. and The PyTorch Lightning team. PyTorch Lightning, March 2019. URL <https://github.com/Lightning-AI/lightning>.
- Fortuin, V., Baranchuk, D., Rätsch, G., and Mandt, S. Gpvae: Deep probabilistic time series imputation. In *International conference on artificial intelligence and statistics*, pp. 1651–1661. PMLR, 2020.
- Gao, J. and Ribeiro, B. On the equivalence between temporal and static equivariant graph representations. In *International Conference on Machine Learning*, pp. 7052–7076. PMLR, 2022.
- Geng, Z., Pokle, A., Luo, W., Lin, J., and Kolter, J. Z. Consistency models made easy. *arXiv preprint arXiv:2406.14548*, 2024.
- Gu, A. and Dao, T. Mamba: Linear-time sequence modeling with selective state spaces. *arXiv preprint arXiv:2312.00752*, 2023.
- Gu, A., Goel, K., and Ré, C. Efficiently modeling long sequences with structured state spaces. In *The International Conference on Learning Representations (ICLR)*, 2022.
- Harris, C. R., Millman, K. J., van der Walt, S. J., Gommers, R., Virtanen, P., Cournapeau, D., Wieser, E., Taylor, J., Berg, S., Smith, N. J., Kern, R., Picus, M., Hoyer, S., van Kerkwijk, M. H., Brett, M., Haldane, A., del Río, J. F., Wiebe, M., Peterson, P., Gérard-Marchant, P., Sheppard, K., Reddy, T., Weckesser, W., Abbasi, H., Gohlke, C., and Oliphant, T. E. Array programming with NumPy. *Nature*, 585(7825):357–362, September 2020. doi: 10.1038/s41586-020-2649-2. URL <https://doi.org/10.1038/s41586-020-2649-2>.
- Ho, J., Jain, A., and Abbeel, P. Denoising diffusion probabilistic models. *Advances in neural information processing systems*, 33:6840–6851, 2020.
- Karras, T., Aittala, M., Aila, T., and Laine, S. Elucidating the design space of diffusion-based generative models. *Advances in neural information processing systems*, 35: 26565–26577, 2022.
- Li, S. C.-X. and Marlin, B. M. A scalable end-to-end gaussian process adapter for irregularly sampled time series classification. *Advances in neural information processing systems*, 29, 2016.
- Li, Y., Yu, R., Shahabi, C., and Liu, Y. Diffusion convolutional recurrent neural network: Data-driven traffic forecasting. In *International Conference on Learning Representations*, 2018. URL <https://openreview.net/forum?id=SJiHXGWAZ>.
- Lipton, Z. C., Kale, D. C., Wetzell, R., et al. Modeling missing data in clinical time series with rnns. *Machine Learning for Healthcare*, 56(56):253–270, 2016.
- Liu, L., Jiang, H., He, P., Chen, W., Liu, X., Gao, J., and Han, J. On the variance of the adaptive learning rate and beyond. *arXiv preprint arXiv:1908.03265*, 2019.
- Liu, M., Huang, H., Feng, H., Sun, L., Du, B., and Fu, Y. Pristi: A conditional diffusion framework for spatiotemporal imputation. In *2023 IEEE 39th International Conference on Data Engineering (ICDE)*, pp. 1927–1939. IEEE, 2023.
- Lu, C. and Song, Y. Simplifying, stabilizing and scaling continuous-time consistency models. *arXiv preprint arXiv:2410.11081*, 2024.

- Luo, S., Tan, Y., Huang, L., Li, J., and Zhao, H. Latent consistency models: Synthesizing high-resolution images with few-step inference. *arXiv preprint arXiv:2310.04378*, 2023.
- Merkel, D. Docker: lightweight linux containers for consistent development and deployment. *Linux journal*, 2014 (239):2, 2014.
- Miao, X., Wu, Y., Wang, J., Gao, Y., Mao, X., and Yin, J. Generative semi-supervised learning for multivariate time series imputation. In *Proceedings of the AAAI conference on artificial intelligence*, volume 35, pp. 8983–8991, 2021.
- Moor, M., Horn, M., Bock, C., Borgwardt, K., and Rieck, B. Path imputation strategies for signature models. In *ICML Workshop on the Art of Learning with Missing Values (Artemiss)*, 2020.
- Mulyadi, A. W., Jun, E., and Suk, H.-I. Uncertainty-aware variational-recurrent imputation network for clinical time series. *IEEE Transactions on Cybernetics*, 52(9):9684–9694, 2021.
- pandas development team, T. pandas-dev/pandas: 1.4.4, February 2020. URL <https://doi.org/10.5281/zenodo.3509134>.
- Paszke, A., Gross, S., Chintala, S., Chanan, G., Yang, E., DeVito, Z., Lin, Z., Desmaison, A., Antiga, L., and Lerer, A. Automatic differentiation in pytorch. In *NIPS-W*, 2017.
- Reyna, M. A., Josef, C., Seyedi, S., Jeter, R., Shashikumar, S. P., Westover, M. B., Sharma, A., Nemat, S., and Clifford, G. D. Early prediction of sepsis from clinical data: the physionet/computing in cardiology challenge 2019. In *2019 Computing in Cardiology (CinC)*, pp. Page–1. IEEE, 2019.
- Rombach, R., Blattmann, A., Lorenz, D., Esser, P., and Ommer, B. High-resolution image synthesis with latent diffusion models. In *Proceedings of the IEEE/CVF conference on computer vision and pattern recognition*, pp. 10684–10695, 2022.
- Ronneberger, O., Fischer, P., and Brox, T. U-net: Convolutional networks for biomedical image segmentation. In *Medical image computing and computer-assisted intervention—MICCAI 2015: 18th international conference, Munich, Germany, October 5-9, 2015, proceedings, part III 18*, pp. 234–241. Springer, 2015.
- Sanchez-Lopez, J. E., Solís-García, J., and Riquelme, J. C. Semi-real-time decision tree ensemble algorithms for very short-term solar irradiance forecasting. *International Journal of Electrical Power & Energy Systems*, 158:109947, 2024.
- Solís-García, J., Vega-Márquez, B., Nepomuceno, J. A., Riquelme-Santos, J. C., and Nepomuceno-Chamorro, I. A. Comparing artificial intelligence strategies for early sepsis detection in the icu: an experimental study. *Applied Intelligence*, 53(24):30691–30705, 2023.
- Solís-García, J., Vega-Márquez, B., Nepomuceno, J. A., and Nepomuceno-Chamorro, I. A. Timba: Time series imputation with bi-directional mamba blocks and diffusion models. *arXiv preprint arXiv:2410.05916*, 2024.
- Song, Y. and Dhariwal, P. Improved techniques for training consistency models. In *The Twelfth International Conference on Learning Representations*, 2024. URL <https://openreview.net/forum?id=WNzy9bRDvG>.
- Song, Y., Sohl-Dickstein, J., Kingma, D. P., Kumar, A., Ermon, S., and Poole, B. Score-based generative modeling through stochastic differential equations. In *International Conference on Learning Representations*, 2021. URL <https://openreview.net/forum?id=PxtTIG12RRHS>.
- Song, Y., Dhariwal, P., Chen, M., and Sutskever, I. Consistency models. In Krause, A., Brunskill, E., Cho, K., Engelhardt, B., Sabato, S., and Scarlett, J. (eds.), *Proceedings of the 40th International Conference on Machine Learning Research*, pp. 32211–32252. PMLR, 23–29 Jul 2023. URL <https://proceedings.mlr.press/v202/song23a.html>.
- Suo, Q., Yao, L., Xun, G., Sun, J., and Zhang, A. Recurrent imputation for multivariate time series with missing values. In *2019 IEEE international conference on healthcare informatics (ICHI)*, pp. 1–3. IEEE, 2019.
- Tashiro, Y., Song, J., Song, Y., and Ermon, S. CSDI: Conditional score-based diffusion models for probabilistic time series imputation. *Advances in Neural Information Processing Systems*, 34:24804–24816, 2021.
- Thanh-Tung, H. and Tran, T. Catastrophic forgetting and mode collapse in gans. In *2020 international joint conference on neural networks (ijcnn)*, pp. 1–10. IEEE, 2020.
- Van Rossum, G. and Drake, F. L. *Python 3 Reference Manual*. CreateSpace, Scotts Valley, CA, 2009. ISBN 1441412697.
- Wes McKinney. Data Structures for Statistical Computing in Python. In Stéfan van der Walt and Jarrod Millman (eds.), *Proceedings of the 9th Python in Science Conference*, pp. 56 – 61, 2010. doi: 10.25080/Majora-92bf1922-00a.
- White, I. R., Royston, P., and Wood, A. M. Multiple imputation using chained equations: issues and guidance for practice. *Statistics in medicine*, 30(4):377–399, 2011.

- Wu, X., Mattingly, S., Mirjafari, S., Huang, C., and Chawla, N. V. Personalized imputation on wearable-sensory time series via knowledge transfer. In *Proceedings of the 29th ACM International Conference on Information & Knowledge Management*, pp. 1625–1634, 2020.
- Wu, Z., Pan, S., Long, G., Jiang, J., and Zhang, C. Graph wavenet for deep spatial-temporal graph modeling. In *Proceedings of the Twenty-Eighth International Joint Conference on Artificial Intelligence, IJCAI-19*, pp. 1907–1913. International Joint Conferences on Artificial Intelligence Organization, 7 2019a. doi: 10.24963/ijcai.2019/264. URL <https://doi.org/10.24963/ijcai.2019/264>.
- Wu, Z., Pan, S., Long, G., Jiang, J., and Zhang, C. Graph wavenet for deep spatial-temporal graph modeling. *arXiv preprint arXiv:1906.00121*, 2019b.
- Yadan, O. Hydra - a framework for elegantly configuring complex applications. Github, 2019. URL <https://github.com/facebookresearch/hydra>.
- Yi, X., Zheng, Y., Zhang, J., and Li, T. St-mvl: Filling missing values in geo-sensory time series data. In *Proceedings of the 25th International Joint Conference on Artificial Intelligence*, 2016.
- Yu, H.-F., Rao, N., and Dhillon, I. S. Temporal regularized matrix factorization for high-dimensional time series prediction. *Advances in neural information processing systems*, 29, 2016.
- Yun, T., Jung, H., and Son, J. Imputation as inpainting: Diffusion models for spatiotemporal data imputation. 2023.

A. Implementation details

A.1. Detailed algorithms description

As an additional detail to the discussion in Section 3.2, the noise scheduler used in this study is based on the Karras scheduler (Karras et al., 2022), with noise levels $\sigma_i \in \{0.002, 80\}$. The magnitude of σ_i and the perturbed input $\tilde{\mathbf{X}}_{t,\sigma_i}$ can vary significantly when passed to the model. Therefore, even though it is not always explicitly mentioned in other studies or equations, these inputs are typically scaled for training the neural network responsible for learning the consistency function. Consequently, the inputs are modulated as follows:

$$\mathbf{F}_\theta(c_{\text{in}}(\sigma_i) \cdot \tilde{\mathbf{X}}_{t,\sigma_i}, \mathcal{X}_t, \mathcal{A}, \tilde{\mathbf{M}}_t, c_{\text{noise}}(\sigma_i)) \quad (7)$$

which, following prior work (Karras et al., 2022; Song et al., 2023; Geng et al., 2024), is implemented in this paper as:

$$c_{\text{in}}(\sigma) = \frac{1}{\sqrt{\sigma^2 + \sigma_{\text{data}}^2}}, \quad c_{\text{in}}(\sigma) = \frac{\ln(\sigma)}{4} \quad (8)$$

To implement the proposed model, we employ two distinct algorithms: one for training (Algorithm 1) and another for sampling or imputation (Algorithm 2).

A.1.1. TRAINING ALGORITHM

The training algorithm has a noteworthy feature: it is optimized to skip a forward pass when $\sigma = \sigma_{\text{min}}$. This optimization slightly accelerates execution for small values of N , although its impact diminishes as training progresses and N increases.

Algorithm 1 Training algorithm

Input: Dataset \mathcal{D} , initial model parameters θ , total steps K , curriculum scheduler $N(k)$, discrete Lognormal distribution $p(N)$, Pseudo-Huber metric $d(\cdot, \cdot)$ and weighting function $\lambda(\cdot)$

Init: $k = 0$

repeat

Sample $(\tilde{\mathbf{X}}_t, \tilde{\mathbf{M}}_t, \mathbf{M}_t, \mathcal{A}_t) \sim \mathcal{D}$, $N \sim p(k)$, $i \sim p(N)$, $\epsilon \sim \mathcal{N}(0, 1)$.

Compute $\tilde{\mathbf{X}}_{t,\sigma_i} = \tilde{\mathbf{X}}_t + \sigma_i \cdot \epsilon$, $\tilde{\mathbf{X}}_{t,\sigma_{i+1}} = \tilde{\mathbf{X}}_t + \sigma_{i+1} \cdot \epsilon$, $\mathcal{X}_t \leftarrow \text{Linear_interpolation}(\tilde{\mathbf{X}}_t)$

if $\sigma_i \neq \sigma_{\text{min}}$ **then**

$\mathcal{L}(\theta) \leftarrow \mathbf{M}_t \cdot \lambda(\sigma_i) d(\mathbf{f}_\theta(\tilde{\mathbf{X}}_{t,\sigma_{i+1}}, \mathcal{X}_t, \mathcal{A}, \tilde{\mathbf{M}}_t, \sigma_{i+1}), \mathbf{f}_{\theta^-}(\tilde{\mathbf{X}}_{t,\sigma_i}, \mathcal{X}_t, \mathcal{A}, \tilde{\mathbf{M}}_t, \sigma_i))$

\mathbf{f}_{θ^-} is done with stopgrad

else

$\mathcal{L}(\theta) \leftarrow \mathbf{M}_t \cdot \lambda(\sigma_i) d(\mathbf{f}_\theta(\tilde{\mathbf{X}}_{t,\sigma_{i+1}}, \mathcal{X}_t, \mathcal{A}, \tilde{\mathbf{M}}_t, \sigma_{i+1}), \tilde{\mathbf{X}}_t)$

end if

$k \leftarrow k + 1$

until $k = K$

A.1.2. SAMPLING ALGORITHM

The sampling algorithm supports sampling in as many steps as desired, however in this article we have focused on 1-step and 2-step sampling. By default, sampling begins from the highest noise level allowed, $\sigma_{i_1} = \sigma_{\text{max}} = 80$. For two-step sampling, a dataset-specific noise level σ_{i_2} is experimentally determined (details in Appendix A.2).

A.2. Hyperparameters

This section provides a detailed overview of the hyperparameters used in CoSTI. First, we list the hyperparameters that were kept constant throughout all experiments conducted in this study:

Algorithm 2 Sampling algorithm

Input: Consistency model $f_{\theta}(\cdot, \cdot)$, sequence of noise levels $\sigma_{i_1} > \sigma_{i_2} > \dots > \sigma_{i_N}$, data to impute \tilde{X}_t , binary missing mask M_t , adjacency matrix \mathcal{A}_t

Init: $S \leftarrow \{\}$ *Set to collect imputations*

Compute $\mathcal{X} \leftarrow \text{Linear_interpolation}(\tilde{X}_t)$

for $j = 1$ **to** 100 **do**

Sample $\epsilon \sim \mathcal{N}(0, 1)$

$\tilde{X}_{t, \sigma_{i_1}} \leftarrow \tilde{X}_t + \sigma_{i_1} \cdot \epsilon$

$\hat{X}_t \leftarrow f_{\theta}(\tilde{X}_{t, \sigma_{i_1}}, \mathcal{X}_t, \mathcal{A}_t, M_t, \sigma_{i_1})$

for $k = 2$ **to** N **do**

Sample $\epsilon \sim \mathcal{N}(0, 1)$

$\hat{X}_t \leftarrow [\tilde{X}_t \odot M_t + \hat{X}_t \odot (1 - M_t)]$ *keep only missing values*

$\tilde{X}_{t, \sigma_{i_k}} \leftarrow \hat{X}_t + \sigma_{i_k} \cdot \epsilon$

$\hat{X}_t \leftarrow f_{\theta}(\tilde{X}_{t, \sigma_{i_k}}, \mathcal{X}_t, \mathcal{A}_t, \tilde{M}_t, \sigma_{i_k})$

end for

Add \hat{X}_t to S : $S \leftarrow S \cup \{\hat{X}_t\}$

end for

$\hat{X}_t \leftarrow \text{Median}(S)$ *Final imputation from median of 100 samples*

- Batch size: 16
- Learning rate: 2.5e-3
- Channel size d : 64
- Number of attention heads: 8
- NEM layers: 4
- σ_{max} : 80
- σ_{min} : 0.002
- σ_{data} : 0.5
- Dropout: 0.2
- c : 5.4e-4
- ρ : 7
- s_0 : 10
- s_1 : 200
- weight decay: 1e-6

Table 5 summarizes the hyperparameters that varied across different datasets and evaluation scenarios.

Table 5. Hyperparameters of CoSTI for each dataset used in this study

Models	AQI-36	METR-LA		PEMS-BAY		Physionet Challenge 2019
		Block	Point	Block	Point	
Time length L	36	24	24	24	24	48
Epochs	200	300	300	150	150	50
f_t	2	2	1	2	1	2
f_s	2	9	9	5	5	2
σ_{i_2}	20.92	0.621	0.821	1.526	5.23	20.92

A.3. Additional Dataset Information

Table 6 provides detailed information about the datasets used in this study, including the topology of their adjacency matrices, the number of nodes and edges, and the proportions of original and additionally injected missing values.

The datasets employed in this study are publicly available and free to use. Specifically, the Torch SpatioTemporal library (Cini & Marisca, 2022) offers tools to download and preprocess the AQI-36, METR-LA, and PEMS-BAY datasets. The Physionet Challenge 2019 dataset is accessible at: <https://physionet.org/content/challenge-2019/1.0.0/>.

Table 6. Graph topology and missing value statistics for each dataset.

Dataset	Graph			N. Neighbors			% Missing Values	
	Type	Nodes	Edges	Mean	Median	Isolated Nodes	Original	Additional Injected
AQI-36	undirected	36	343	19.06	24.5	0	13.24	11.33
METR-LA (P)	directed	207	1515	7.32	7.0	5	8.10	23.00
(B)	-	-	-	-	-	-	-	8.4
PEMS-BAY (P)	directed	325	2369	7.29	7.0	12	0.02	25.0
(B)	-	-	-	-	-	-	-	9.07
Physionet Challenge 2019	undirected	40	752	37.6	38	0	78.43	5.39

A.4. Code Reproducibility

This study emphasizes code reproducibility and accessibility to the datasets employed. The implementation has been made publicly available on GitHub: <https://github.com/javiersgjavico/CoSTI>.

The codebase is written in Python (Van Rossum & Drake, 2009) and leverages several widely used open-source libraries, including:

- Pytorch (Paszke et al., 2017).
- Pytorch Lightning (Falcon & The PyTorch Lightning team, 2019)
- Numpy (Harris et al., 2020).
- Torch spatio-temporal (Cini & Marisca, 2022).
- Pandas (pandas development team, 2020; Wes McKinney, 2010).
- Hydra (Yadan, 2019).

To streamline the execution of experiments, a Docker image and corresponding container (Merkel, 2014) were created, along with scripts to facilitate their setup and use. All experimental results were obtained using a system configured as follows: Ubuntu 22.04.2 LTS operating system, an AMD Ryzen Threadripper PRO 3955WX CPU with 16 cores, an NVIDIA RTX A5000 GPU with 24 GB of memory, and 128 GB of DDR4 RAM (8x16 GB modules). Table 7 summarizes the training and inference times achieved with this setup.

Table 7. Training and inference times measured in hours.

Models	AQI-36		METR-LA		PEMS-BAY		Physionet Challenge 2019	
	Training	Inference	Training	Inference	Training	Inference	Training	Inference
CSDI	1.17	0.22	43.67	1.74	114.67	4.62	7.35	8.16
PriSTI	1.61	0.33	49.25	2.44	118.33	5.99	13.13	15.87
TIMBA	0.56	0.44	77.00	3.65	196.42	8.71	15.03	18.19
CoSTI	1.99	0.005	79.42	0.06	108.75	0.16	12.92	0.48

B. Additional Results

B.1. Benchmark analysis

To provide a broader context for the results obtained with CoSTI compared to other imputation techniques, we evaluated it using the comprehensive benchmark introduced by Cini et al. (2022). This benchmark includes a diverse range of methods, encompassing both traditional statistical approaches and more advanced generative models. Specifically, it evaluates the following categories of techniques:

1. **Statistical techniques:** Methods based on simple aggregations, such as MEAN (historical average values), DA (daily averages), and KNN (proximity-based imputation).
2. **Machine Learning Algorithms:** These include Lin-ITP (linear interpolation), MICE (White et al., 2011) (multiple imputations), VAR (vector autoregressive models), and KF (Kalman Filter).
3. **Matrix Factorization Techniques:** TRMF (Yu et al., 2016) (temporal regularized matrix factorization) and BATF (Chen et al., 2019) (Bayesian augmented tensor factorization).
4. **Autoregressive Models:** These include BRITS (Cao et al., 2018), MPGRU (a GNN-based predictor resembling DCRNN (Li et al., 2018), and GRIN (Cini et al., 2022).
5. **Generative Models:** Advanced generative techniques, such as CSDI, PriSTI, TIMBA, V-RIN (Mulyadi et al., 2021) (a VAE with uncertainty quantification), GP-VAE (Fortuin et al., 2020) (a combination of VAEs and Gaussian processes), and rGAIN (Miao et al., 2021) (GAN-based imputation with recurrent structures).

The detailed evaluation results, summarized in Table 8, highlight the strong performance of diffusion-based approaches such as CSDI, PriSTI, and TIMBA. Notably, CoSTI achieves comparable or superior results in multiple cases, demonstrating its ability to harness the strengths of diffusion models, particularly their capacity to outperform traditional methods like autoregressive techniques (Tashiro et al., 2021).

Table 8. Performance comparison of CoSTI with existing methods from the benchmark established in the literature (Cini et al., 2022). Results are presented in terms of MAE and MSE, providing a comprehensive evaluation of imputation accuracy. The best value is highlighted in bold, and any case where CoSTI outperforms a DDPM model is underlined.

Models	AQI-36		METR-LA				PEMS-BAY			
	Simulated failure (24.6%)		Block-missing (16.6%)		Point-missing (31.1%)		Block-missing (9.2%)		Point-missing (25.0%)	
	MAE	MSE	MAE	MSE	MAE	MSE	MAE	MSE	MAE	MSE
Mean	53.48 ± 0.00	4578.08 ± 0.00	7.48 ± 0.00	139.54 ± 0.00	7.56 ± 0.00	142.22 ± 0.00	5.46 ± 0.00	87.56 ± 0.00	5.42 ± 0.00	86.59 ± 0.00
DA	50.51 ± 0.00	4416.10 ± 0.00	14.53 ± 0.00	445.08 ± 0.00	14.57 ± 0.00	448.66 ± 0.00	3.30 ± 0.00	43.76 ± 0.00	3.35 ± 0.00	44.50 ± 0.00
KNN	30.21 ± 0.00	2892.31 ± 0.00	7.79 ± 0.00	124.61 ± 0.00	7.88 ± 0.00	129.29 ± 0.00	4.30 ± 0.00	49.90 ± 0.00	4.30 ± 0.00	49.80 ± 0.00
Lin-ITP	14.46 ± 0.00	673.92 ± 0.00	3.26 ± 0.00	33.76 ± 0.00	2.43 ± 0.00	14.75 ± 0.00	1.54 ± 0.00	14.14 ± 0.00	0.76 ± 0.00	1.74 ± 0.00
KF	54.09 ± 0.00	4942.26 ± 0.00	16.75 ± 0.00	534.69 ± 0.00	16.66 ± 0.00	529.96 ± 0.00	5.64 ± 0.00	93.19 ± 0.00	5.68 ± 0.00	93.32 ± 0.00
MICE	30.37 ± 0.09	2594.06 ± 7.17	4.22 ± 0.05	51.07 ± 1.25	4.42 ± 0.07	55.07 ± 1.46	2.94 ± 0.02	28.28 ± 0.37	3.09 ± 0.02	31.43 ± 0.41
VAR	15.64 ± 0.08	833.46 ± 13.85	3.11 ± 0.08	28.00 ± 0.76	2.69 ± 0.00	21.10 ± 0.02	2.09 ± 0.10	16.06 ± 0.73	1.30 ± 0.00	6.52 ± 0.01
TRMF	15.46 ± 0.06	1379.05 ± 34.83	2.96 ± 0.00	22.65 ± 0.13	2.86 ± 0.00	20.39 ± 0.02	1.95 ± 0.01	11.21 ± 0.06	1.85 ± 0.00	10.03 ± 0.00
BATF	15.21 ± 0.27	662.87 ± 29.55	3.56 ± 0.01	35.39 ± 0.03	3.58 ± 0.01	36.05 ± 0.02	2.05 ± 0.00	14.48 ± 0.01	2.05 ± 0.00	14.90 ± 0.06
V-RIN	10.00 ± 0.10	838.05 ± 24.74	6.84 ± 0.17	150.08 ± 6.13	3.96 ± 0.08	49.98 ± 1.30	2.49 ± 0.04	36.12 ± 0.66	1.21 ± 0.03	6.08 ± 0.29
GP-VAE	25.71 ± 0.30	2589.53 ± 59.14	6.55 ± 0.09	122.33 ± 2.05	6.57 ± 0.10	127.26 ± 3.97	2.86 ± 0.15	26.80 ± 2.10	3.41 ± 0.23	38.95 ± 4.16
rGAIN	15.37 ± 0.26	641.92 ± 33.89	2.90 ± 0.01	21.67 ± 0.15	2.83 ± 0.01	20.03 ± 0.09	2.18 ± 0.01	13.96 ± 0.20	1.88 ± 0.02	10.37 ± 0.20
MPGRU	16.79 ± 0.52	1103.04 ± 106.83	2.57 ± 0.01	25.15 ± 0.17	2.44 ± 0.00	22.17 ± 0.03	1.59 ± 0.01	14.19 ± 0.11	1.11 ± 0.00	7.59 ± 0.02
BRITS	14.50 ± 0.35	622.36 ± 65.16	2.34 ± 0.01	17.00 ± 0.14	2.34 ± 0.00	16.46 ± 0.05	1.70 ± 0.01	10.50 ± 0.07	1.47 ± 0.00	7.94 ± 0.03
GRIN	12.08 ± 0.47	523.14 ± 57.17	2.03 ± 0.00	13.26 ± 0.05	1.91 ± 0.00	10.41 ± 0.03	1.14 ± 0.01	6.60 ± 0.10	0.67 ± 0.00	1.55 ± 0.01
CSDI	9.74 ± 0.16	388.37 ± 11.42	1.90 ± 0.01	12.27 ± 0.18	1.77 ± 0.05	9.42 ± 0.47	0.84 ± 0.00	4.06 ± 0.04	0.58 ± 0.00	1.30 ± 0.04
PriSTI	9.84 ± 0.11	376.11 ± 10.62	1.78 ± 0.00	10.64 ± 0.13	1.70 ± 0.00	8.47 ± 0.04	0.87 ± 0.01	4.64 ± 0.21	0.59 ± 0.00	1.61 ± 0.03
TIMBA	9.56 ± 0.4	352.29 ± 5.33	1.76 ± 0.02	10.36 ± 0.34	1.69 ± 0.00	8.36 ± 0.01	0.84 ± 0.01	4.57 ± 0.08	0.58 ± 0.00	1.63 ± 0.08
CoSTI	10.13 ± 0.08	<u>377.48</u> ± 9.29	<u>1.85</u> ± 0.01	<u>11.44</u> ± 0.08	<u>1.76</u> ± 0.01	<u>9.01</u> ± 0.06	0.93 ± 0.03	<u>4.52</u> ± 0.15	0.64 ± 0.01	<u>1.53</u> ± 0.15
CoSTI-2	9.90 ± 0.13	<u>358.67</u> ± 13.05	<u>1.84</u> ± 0.01	<u>11.35</u> ± 0.14	<u>1.75</u> ± 0.00	<u>8.97</u> ± 0.05	0.91 ± 0.02	<u>4.43</u> ± 0.12	0.63 ± 0.01	<u>1.44</u> ± 0.12

These findings emphasize the competitiveness of CoSTI across a diverse benchmark of imputation techniques. While diffusion-based models, including CSDI, PriSTI, and TIMBA, consistently deliver state-of-the-art performance, CoSTI matches their MSE across various datasets and imputation scenarios. However, in certain cases, CoSTI exhibits slightly higher MAE compared to some diffusion-based counterparts, suggesting potential areas for improvement in capturing absolute error dynamics. Despite this, CoSTI demonstrates robust and versatile performance, positioning itself as a strong alternative to leading diffusion-based models, particularly in scenarios where balancing accuracy and speed is crucial.

B.2. Sensitivity analysis

The outcomes of the missing rate experiment described in Section 5.3.2 are summarized for the four models in Tables 9 and 10, reporting performance in terms of MAE and MSE, respectively.

Table 9. Sensitivity analysis for different levels of missing values in the METR-LA dataset under the Point missing scenario, presented in terms of MAE. The best value is highlighted in bold, and any case where CoSTI outperforms a DDPM model is underlined.

MAE - METR-LA (P)									
Models	10%	20%	30%	40%	50%	60%	70%	80%	90%
CSDI	1.77	1.82	1.88	1.96	2.07	2.20	2.39	2.70	3.29
PriSTI	1.64	1.67	1.71	1.76	1.81	1.89	1.99	2.14	2.43
TIMBA	1.64	1.66	1.70	1.75	1.80	1.88	1.98	2.13	2.41
CoSTI	<u>1.69</u>	<u>1.71</u>	<u>1.75</u>	<u>1.80</u>	<u>1.87</u>	<u>1.94</u>	<u>2.03</u>	<u>2.18</u>	<u>2.44</u>

Table 10. Sensitivity analysis for different levels of missing values in the METR-LA dataset under the Point missing scenario, presented in terms of MSE. The best value is highlighted in bold, and any case where CoSTI outperforms a DDPM model is underlined.

MSE - METR-LA (P)									
Models	10%	20%	30%	40%	50%	60%	70%	80%	90%
CSDI	8.50	9.10	9.92	10.88	12.14	13.86	16.54	21.75	32.54
PriSTI	7.71	8.07	8.61	9.29	10.08	11.24	12.88	15.88	22.08
TIMBA	7.60	7.91	8.48	9.15	9.96	11.09	12.65	15.55	21.57
CoSTI	<u>7.95</u>	<u>8.31</u>	<u>8.89</u>	<u>9.63</u>	<u>10.54</u>	<u>11.67</u>	<u>13.22</u>	<u>16.22</u>	<u>21.77</u>

B.3. Ablation Study and Component Analysis

This section provides a comprehensive evaluation of our model through ablation studies and component analysis. We investigate the contribution of the techniques introduced in this paper, examining the impact of architectural components, curriculum learning strategies, and optimizers.

B.3.1. ARCHITECTURAL COMPONENT ABLATIONS

We conducted the following experiments to analyze the impact of architectural components:

- **w/o Cond:** This experiment evaluates the performance of CoSTI when the second model head, responsible for extracting conditional information, is removed.
- **w/o SFTE:** This test assesses the model’s performance when the STFEM modules, which extract spatio-temporal representations of the input sequence at the network’s entry, are omitted.
- **w/o NEM:** This experiment examines the impact of removing the NEM blocks, located at the core of the network, that are designed to estimate noise in the input sequence.
- **w/o self-attention:** This test evaluates the contribution of the Bi-Mamba and Spatial Self-Attention layers within the NEM blocks to assess whether their inclusion enhances performance.

Table 11. Performance comparison (MAE and MSE) of CoSTI and its ablated versions across datasets.

Dataset	MAE	MSE
CoSTI	1.76 ± 0.01	9.01 ± 0.06
w/o Cond	6.36 ± 0.02	153.51 ± 1.89
w/o STFE	2.33 ± 0.06	16.32 ± 0.99
w/o NEM	1.77 ± 0.01	9.17 ± 0.05
w/o self-attention	1.77 ± 0.01	9.14 ± 0.14

The results in Table 11 demonstrate the contributions of the components evaluated through the ablation study. The removal of the conditional head (**w/o Cond**) results in the largest performance degradation, with substantial increases in both MAE and MSE. This highlights the importance of the conditional information captured by this head, which appears crucial for the model’s ability to make accurate predictions. Similarly, excluding the STFEM module (**w/o SFTE**) considerably worsens performance, indicating that the spatio-temporal representations extracted by this module are fundamental for capturing the input sequence’s underlying structure.

In the case of the NEM blocks (**w/o NEM**), their removal causes a slight performance decline, which suggests that noise estimation primarily contributes to refining the model’s predictions but is not as critical as other components. Likewise, excluding the self-attention mechanism (**w/o self-attention**) leads to marginally higher MAE and MSE. Although the difference is small, this indicates that the Bi-Mamba and Spatial Self-Attention layers enhance the model’s ability to focus on relevant spatio-temporal features, leading to slightly better performance. These results collectively emphasize that each component, even those with smaller individual contributions, plays a role in improving the model’s overall robustness and precision.

B.3.2. CURRICULUM LEARNING STRATEGY EVALUATION

In this section, we explore various curriculum learning schedulers to evaluate their impact on model performance, with a graphical representation of some of the tested schedulers provided in Figure 4.

- **CoSTI Scheduler:** This is the scheduler implemented in this paper. It is a linear scheduler with $s_0 = 10$ and $s_1 = 200$. In Table 12 and Figure 4, it is labeled as “Linear $s_0 = 10$.”
- **Linear $s_0 = 2$:** This scheduler is similar to the one implemented in this paper but uses $s_0 = 2$.
- **Linear $s_1 = 1280$:** This scheduler also follows a linear approach, but with $s_0 = 10$ and $s_1 = 1280$, as proposed in Song & Dhariwal (2024).
- **Original Scheduler:** This scheduler is the one originally proposed in Song et al. (2023), with $s_0 = 2$ and $s_1 = 200$.
- **Constant:** This is the simplest scheduler, where $N = 200$ remains constant throughout training.
- **Exponential:** Proposed in Song & Dhariwal (2024), this scheduler increases N exponentially until reaching the target value, with $s_0 = 10$ and $s_1 = 200$.
- **Pretrain + Exponential:** This is a custom scheduler that introduces a pretraining phase with $N = 2$. Inspired by Geng et al. (2024), this phase aims to train the model to generate accurate imputations for MTS starting from pure noise by comparing the noisy input with the original unperturbed sample. This process helps the model learn to predict correct imputations before being trained for consistency across different σ values. After this pretraining phase, it is an exponential scheduler with $s_0 = 10$ and $s_1 = 200$. The pretraining phase comprises $r = 1/3$ of the total steps, followed by the exponential scheduler.

The results in Table 12 highlight why the linear scheduler with $s_0 = 10$ and $s_1 = 200$ achieves such competitive performance, even when compared to more elaborate approaches like exponential growth or pretraining-based strategies. This success stems from the same principles that motivate these advanced techniques: a progressive improvement in model performance as N increases. While larger N values reduce approximation bias and improve imputation quality, they can also introduce higher variance or instability during training (Song & Dhariwal, 2024; Geng et al., 2024). The linear scheduler effectively balances this trade-off by providing a gradual, steady increase in N . Unlike exponential approaches, which can transition too aggressively, the linear strategy ensures that each N range is explored sufficiently, allowing the model to adapt to incremental increases in difficulty without destabilizing the training process.

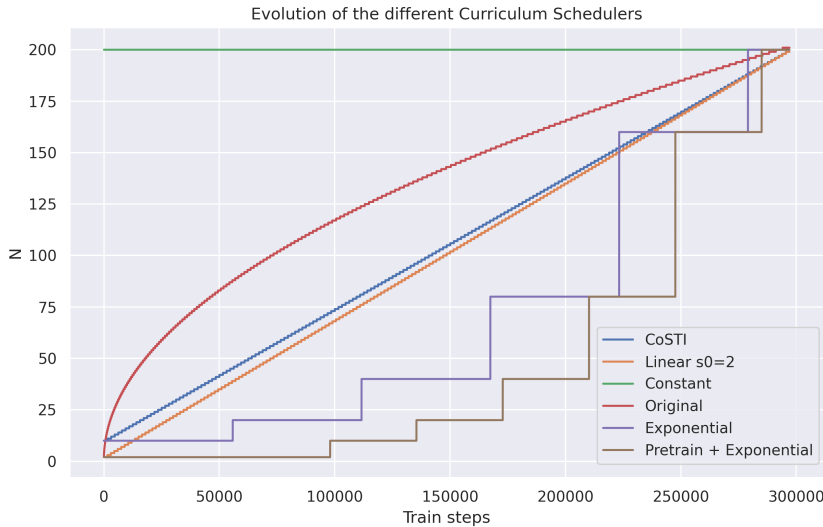


Figure 4. Graphical representation of selected Curriculum Schedulers evaluated in this experiment.

Table 12. Performance results for different curriculum learning schedulers.

Dataset	MAE	MSE
Linear $s_0 = 10$ (CoSTI)	1.76 \pm 0.01	9.01 \pm 0.06
Linear $s_0 = 2$	1.87 \pm 0.05	10.01 \pm 0.43
Linear $s_1 = 1280$	1.82 \pm 0.01	9.46 \pm 0.19
Constant	1.86 \pm 0.03	9.30 \pm 0.29
Original	1.80 \pm 0.02	9.30 \pm 0.28
Exponential	1.79 \pm 0.03	9.44 \pm 0.41
Pretrain + Exponential	1.79 \pm 0.03	9.18 \pm 0.07

Furthermore, the simplicity of the linear scheduler is a significant advantage. More complex strategies, such as pretraining followed by exponential growth, introduce additional design considerations, such as determining pretraining duration or tuning exponential rates. By contrast, the linear scheduler only requires setting an initial and final value for N . This simplicity reduces the risk of implementation errors and minimizes the burden of hyperparameter tuning, making it a practical choice for real-world applications. Additionally, starting at $N = 10$ offers a moderate initial difficulty level that allows the model to learn foundational patterns effectively before progressing to more complex tasks. We theorize that this moderate starting point strikes a good balance between simplicity and effectiveness, ensuring a smooth progression during training.

While exponential and pretraining strategies have strong theoretical justifications, the linear scheduler with $s_0 = 10$ and $s_1 = 200$ demonstrates that simplicity and stability can often yield equally strong — if not superior — results. Its gradual and controlled progression strikes an effective balance between bias and variance, ensuring robust model adaptation throughout training. This combination of simplicity and progressive adaptation makes the linear approach not only a competitive alternative but also a reliable and efficient solution for MTSI tasks.

B.3.3. OPTIMIZER PERFORMANCE COMPARISON

In this section, we compare the original optimizer used in our experiments, **AdamWScheduleFree** (Defazio et al., 2024), with two alternative configurations widely used in the literature:

- **RAdam**: This optimizer is commonly employed in papers on Consistency Models (Song et al., 2023; Song & Dhariwal, 2024; Geng et al., 2024). The configuration uses the RAdam optimizer (Liu et al., 2019) without learning rate decay, warm-up, or weight decay. The learning rate is set to $1e-4$, as suggested in Song & Dhariwal (2024).
- **AdamW + MultiStepLR**: This configuration is used in models such as CSDI, PriSTI, and TIMBA. It combines AdamW with a learning rate of $1e-3$ and weight decay of $1e-6$. Additionally, it employs a MultiStepLR schedule, reducing the learning rate to $1e-4$ and $1e-5$ when 75% and 90% of training epochs are completed, respectively.

The comparison of optimizers highlights the efficacy of the proposed AdamWScheduleFree configuration in achieving superior quantitative performance and maintaining training stability. As shown in Table 13, AdamWScheduleFree consistently outperforms the alternatives, achieving the lowest MAE and MSE across experiments. While AdamW achieves slightly better results than RAdam, its reliance on a complex learning rate schedule introduces additional hyperparameter tuning overhead, which is avoided by the simpler, schedule-free design of AdamWScheduleFree.

Table 13. Performance results for different optimizers.

Dataset	MAE	MSE
AdamWScheduleFree (CoSTI)	1.76 \pm 0.01	9.01 \pm 0.06
RAdam	1.84 \pm 0.02	9.99 \pm 0.31
AdamW	1.81 \pm 0.02	9.41 \pm 0.14

Figure 5 provides further insights into the training dynamics. AdamWScheduleFree achieves smoother and more consistent convergence in both training and validation loss curves, maintaining a lower imputation error on the validation set (measured in MAE) throughout the training process. The progressive smoothing of the training loss can be attributed to the curriculum learning strategy employed. By incrementally increasing the number of N , the PF-FLOW comparisons are progressively localized to closer points, which reduces the complexity of the task over time. This design allows the model to gradually refine its predictions, leading to a steady and significant reduction in training loss.

Overall, these results demonstrate that AdamWScheduleFree simplifies the optimization process while delivering state-of-the-art performance. Its ability to achieve competitive results highlights its effectiveness and practicality for imputation tasks, making it a strong alternative to more complex configurations.

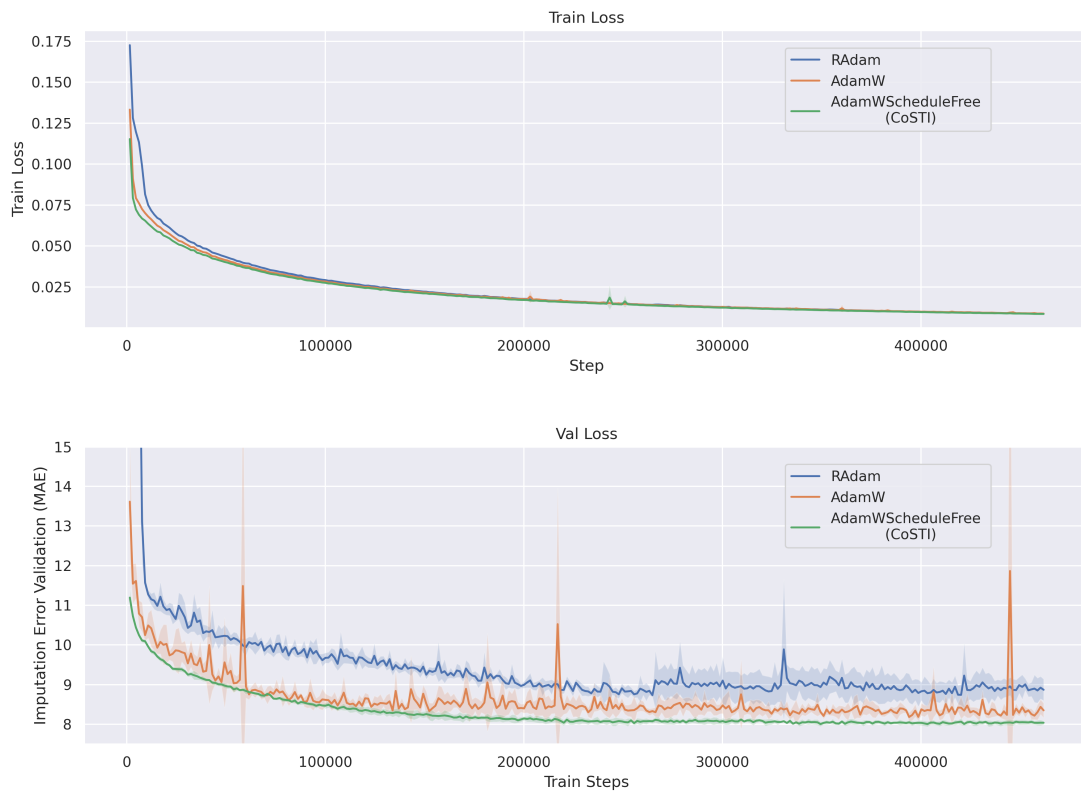


Figure 5. Training and validation loss curves for the optimizer comparison experiment. Shaded regions indicate the mean and standard deviation across five runs, illustrating the consistency and variability of each optimizer’s performance.